

Calculation of the exposure of GRANDProto300 to cosmic rays

Sei Kato,^{a,*} Clément Prévotat^a and Rafael Alves Batista^{a,b} for the GRAND Collaboration

(a complete list of authors can be found at the end of the proceedings)

^a*Institut d'Astrophysique de Paris, CNRS UMR 7095, Sorbonne Université, Paris, France*

^b*Laboratoire de Physique Nucléaire et des Hautes Energies, Sorbonne Université, Paris, France*

E-mail: sei.kato@iap.fr

GRANDProto300 is one of the prototype experiments of the Giant Radio Array for Neutrino Detection. It will feature about 300 radio antenna detectors in Xiaodushang in Dunhuang, China, covering a total geometrical area of about 200 km². A main scientific goal of GRANDProto300 is the study of cosmic rays in the transition region ($10^{17} \text{ eV} < E < 10^{18.5} \text{ eV}$). Our study calculates the exposure of GRANDProto300 to cosmic rays and estimates the number of cosmic-ray events to be detected during a fixed observation period. The trigger efficiency reaches 50, 80, and 90% at $10^{17.5}$, $10^{17.9}$, and $10^{18.3} \text{ eV}$, respectively. The exposure of GRANDProto300 is 50 km² day sr at around $10^{17.5} \text{ eV}$, and the expected number of observed cosmic rays with energies above 10^{17} eV and zenith angles above 65° is about 130 events per day. GRANDProto300 will be able to measure the cosmic-ray energy spectrum in $10^{17.2} \text{ eV} < E < 10^{19.5} \text{ eV}$ through one-year observation, with a statistical precision about five times better than the previous spectral measurement by a mono-fluorescence detector of the Telescope Array Low-Energy Extension. The statistical uncertainty in the measurement of the mean depth of the air-shower maximum X_{max} is about five times better than the previous measurements using radio detectors at $10^{17.5} \text{ eV}$; systematic uncertainties should be a dominant contribution limiting our interpretation of the chemical composition of cosmic rays in the transition region.

39th International Cosmic Ray Conference (ICRC2025)
15–24 July, 2025
Geneva, Switzerland



ICRC 2025

The Astroparticle Physics Conference
Geneva July 15-24, 2025

*Speaker

1. Introduction

The Giant Radio Array for Neutrino Detection (GRAND) is a future radio-antenna-array experiment mainly aiming at the first detection of ultra-high-energy neutrinos well beyond 10^{17} eV and the study of the origin of ultra-high-energy cosmic rays ($E > 10^{18}$ eV) [1, 2]. It will detect the geomagnetic radio emission from Earth-skimming hadronic showers produced by the decay of tau leptons, the products of the charged-current reaction of astrophysical tau neutrinos in the Earth. A main technical challenge of GRAND is an autonomous trigger of radio emission from air showers only using radio detectors. GRAND has three prototype experiments, GRANDProto300 in China, GRAND@Auger in Argentina and GRAND@Nançay in France. In particular, GRANDProto300 (hereafter called GP300) will be dedicated to the calibration of our radio detectors, the validation of the autonomous radio trigger, and the study of cosmic rays (CRs) in the transition region (10^{17} eV $< E < 10^{18.5}$ eV) [3]. This study focuses on the ability of GP300 for the CR observation by calculating the exposure of the array to CRs through a simulation-based study.

2. GRANDProto300 (GP300)

GP300 is a prototype radio-antenna array to be installed in Xiaodushan (40.99°N, 93.94°E, ~1200 m above sea level) in Dunhuang, China. Figure 1 shows the bird's-eye view of GP300. It will make use of 299 radio detector units (DUs) covering a total geometrical area of about 200 km². Each DU has butterfly-shaped steel antenna arms extending in the South-North (X-arm), East-West (Y-arm), and the vertical directions (Z-arm). The X- and Y-arms are dipoles, while the Z-arm is a monopole and the supporting pole works as its second arm. For the detailed description of the DU design and its functionality, see [4]. GP300 has an infill array with an interval of 577 m between DUs, surrounded by a sparse array with an interval of 1 km. The infill array is used to lower the energy threshold for CR events. Motivations of GP300 include the validation of the autonomous trigger of radio emission from CR-induced air showers only using radio detectors and the study of the transition region in the CR energy spectrum above 10^{17} eV.

3. Simulation

This study uses the CoREAS code [5] to simulate the development of CR-induced air showers and calculate the associated radio emission at each position of the GP300 DUs. The CR events are generated following the uniform distribution in the logarithmic energy space within a range of 10^{17} eV $< E < 10^{20}$ eV. The distribution of the incoming directions is uniform in zenith angle θ within $65^\circ < \theta < 88^\circ$ and azimuthal angle ϕ within $0^\circ < \phi < 360^\circ$. Out of total 1.5×10^4 events generated in the simulation, 50% are protons and the remaining 50% are irons. The shower core positions of the events are randomly distributed within the rectangular region enclosed within the black dashed lines shown in Figure 1. The region covers only a partial array, so the current analysis using the simulation data only gives an approximate estimate of exposure. The simulation assuming a large geometrical area enough to cover the entire array will be performed in the future.

To calculate the exposure of GP300 for realistic observations, events are weighted to reproduce the measured energy spectrum of CRs and the isotropic distribution of their incoming directions.

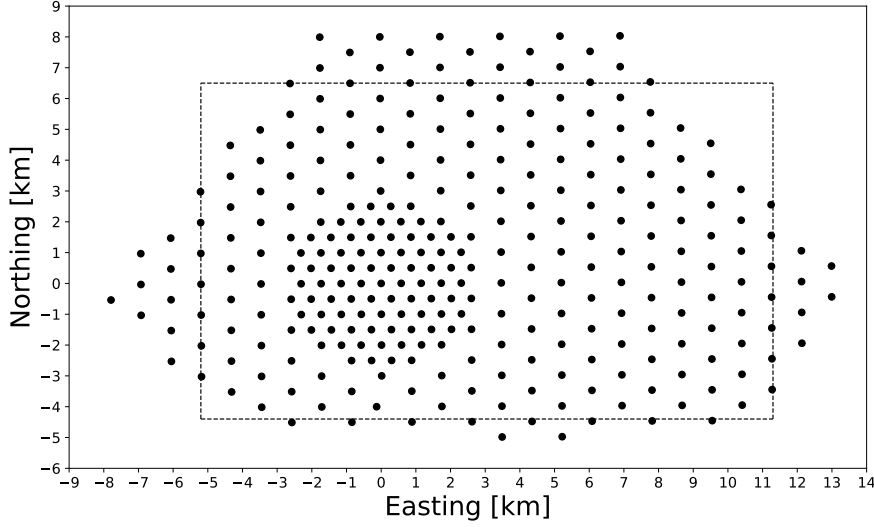


Figure 1: Bird's-eye view of the GP300 radio detector array. The black dashed lines enclose the rectangular region ($[-5.2 \text{ km}, 11.3 \text{ km}]$ in Easting and $[-4.4 \text{ km}, 6.5 \text{ km}]$ in Northing) where the core positions are randomly distributed.

For the CR energy spectrum, this study assumes the best-fit broken power-law function to the spectral measurement by the fluorescence detector of the Telescope Array Low-Energy Extension (TALE) [6]:

$$\frac{dN}{dE} = \begin{cases} J_0 \left(\frac{E}{E_{\text{br}}} \right)^{-2.92} & 10^{17} \text{ eV} < E < E_{\text{br}} \\ J_0 \left(\frac{E}{E_{\text{br}}} \right)^{-3.19} & E_{\text{br}} \leq E < 10^{20} \text{ eV} \end{cases} \quad (1)$$

where $J_0 = 2.27 \times 10^{-16} \text{ km}^{-2} \text{ day}^{-1} \text{ sr}^{-1} \text{ eV}^{-1}$ and $E_{\text{br}} = 10^{17.04} \text{ eV}$.

The radio emission from an air shower event is calculated with CoREAS for the DUs that are located within four Cherenkov radii from the simulated core position of the event. The calculated emission is then processed with GRANDlib [4] to simulate the output signals from the DUs. The time trace of the electric field of the radio emission is converted into the time trace of open circuit voltage by accounting for the antenna effective length. The open circuit voltage trace is then fed into the radio frequency chain of the DUs to obtain the output voltage trace, which is then digitized by the analog-to-digital (ADC) converter. The Galactic noise: the radio synchrotron emission from high-energy galactic electrons, measured by the real experiment for a fixed observation period [7], is added to the simulated ADC trace of the shower radio emission. The amplitude of the Galactic noise in our simulation is 15.1 ADC counts in terms of root mean square (RMS). The value of the noise amplitude is fixed in our simulation analysis, although it fluctuates by a few ADC counts during the operation in the real experiment. For the detailed description of the signal processing in the DUs, see [4].

To discuss the trigger, the Hilbert envelope of the time trace of ADC counts is calculated in each of the three arms of the DUs. The three traces of the Hilbert envelope are summed in quadrature,

and each DU is triggered when the quadrature sum exceeds 90.6 ADC counts. Finally, an overall trigger is issued when any five or more DUs are triggered.

The exposure is calculated from the following equation:

$$\text{Exposure} = A_{\text{geo}} \Omega T_{\text{obs}} \frac{\sum_i N_{\text{trig},i} \cos\theta}{\sum_j N_{\text{sim},j}}, \quad (2)$$

where $A_{\text{geo}} = 180 \text{ km}^2$ is the geometrical area of the region where the shower core positions are distributed (see Figure 1), $\Omega = 2.4 \text{ sr}$ the solid angle of the entire sky region assumed in the simulation, and T_{obs} the observation period. N_{trig} is the number of events that triggered the GP300 array, and N_{sim} is the number of events generated in the simulation. Note that the both numbers of events are weighted as mentioned above so that the generated events follow the TALE CR energy spectrum and the isotropic distribution of incoming direction. The $\cos\theta$ factor in the numerator accounts for the fact that the effective geometrical area is smaller by $\cos\theta$ for an injected CR event with a zenith angle of θ .

4. Results and discussions

The left panel of Figure 2 shows the trigger efficiency of GP300 as a function of energy. The trigger efficiency is defined as a fraction of events that triggered the array to the total events generated in the simulation. The error bars show the statistical errors coming from the statistical uncertainty in the number of triggered events assuming a binomial distribution. The horizontal axis shows true energies of CR events generated in the simulation. The trigger efficiency of GP300 reaches 50, 80, and 90% at $10^{17.5}$, $10^{17.9}$, and $10^{18.3}$ eV, respectively. The right panel of Figure 2 shows the trigger efficiency for three different zenith angle ranges: $65.0^\circ < \theta < 74.5^\circ$, $74.5^\circ < \theta < 81.3^\circ$ and $81.3^\circ < \theta < 88.0^\circ$. As the zenith angle increases, the trigger efficiency improves due to the large footprint size of the radio emission on the ground, which is able to trigger more DUs. On the other hand, threshold energy becomes higher with an increase of θ due to the attenuation of the radio emission from highly inclined showers. The figure shows that the efficiency is determined by the balance between the above two physical processes: the footprint size of the air-shower radio emission and its attenuation as a function of zenith angle.

The left panel of Figure 3 shows the exposure of GP300 as a function of energy for one-day observation calculated from Equation (2) with $T_{\text{obs}} = 1$ day. The exposure reaches 50, 80, and $90 \text{ km}^2 \text{ day sr}$ at $10^{17.5}$, 10^{18} , and 10^{19} eV, respectively. The right panel of Figure 3 shows the expected number of CR events observed by GP300 per day for each energy bin. Integration over the whole energy range in our simulation ($10^{17} \text{ eV} < E < 10^{20} \text{ eV}$ and $65^\circ < \theta < 88^\circ$) gives about 130 events per day.

Figure 4 shows a prediction of the reconstructed CR spectrum from the one-year observation by GP300 compared with the measurement by the TALE fluorescence detector [6]. For our prediction, the horizontal axis presents true energies of CR events generated in the simulation. A total number of 4.9×10^4 CRs will be observed, and the preliminary estimate of the number of CRs in each energy bin is presented in Table 1. Compared with the previous TALE observation comprehensively covering the transition region, GP300 will be able to determine the CR flux with a better statistical precision by a factor of about eight and five at the $10^{17.5}$ eV and 10^{18} eV energy ranges, respectively. In the

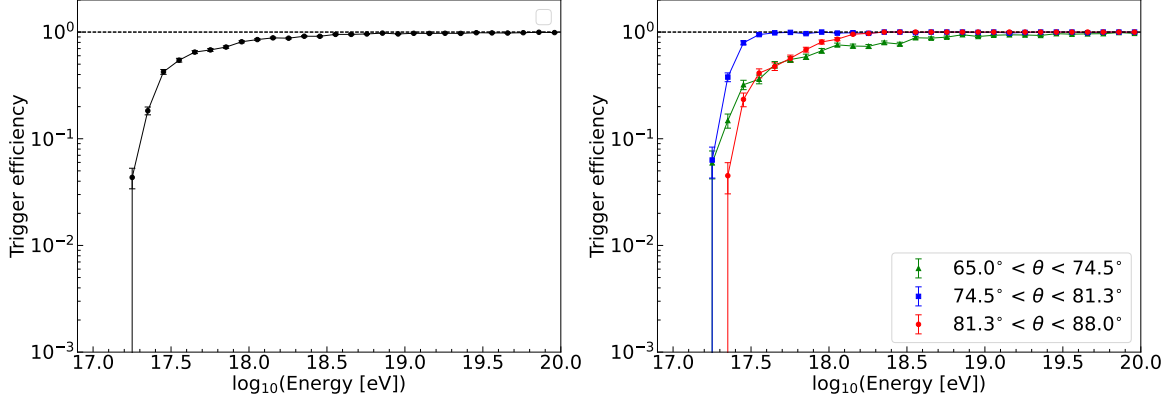


Figure 2: *Left panel:* trigger efficiency as a function of energy of CR events. The error bars are statistical errors assuming a binomial distribution for triggered events. The horizontal black dashed line indicates a 100% efficiency. *Right panel:* trigger efficiency for three different zenith-angle ranges.

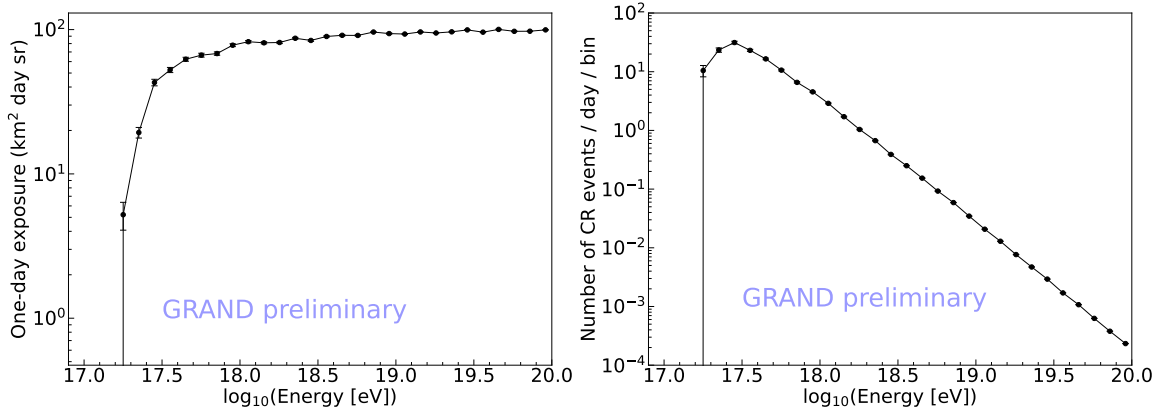


Figure 3: *Left panel:* exposure of GP300 in one-day observation as a function of energy of CR events. The error bars are statistical errors assuming a binomial distribution for triggered events. *Right panel:* expected number of CR events observed by GP300 per day per energy bin.

energy range of $10^{18} \text{ eV} \lesssim E \lesssim 10^{19} \text{ eV}$, the event statistics estimated for the GP300 observation is also comparable with that of the measurement by the dense surface detector array with a 750 m spacing of the Pierre Auger Observatory [8]. The spectrum will be successfully reconstructed up to $10^{19.5} \text{ eV}$ before the steep cutoff of the spectrum [9–11]. Note that our prediction is made from a simple extrapolation of the best-fit power-law function to the TALE observation above 10^{17} eV . The measured CR energy spectrum has an ankle structure at around $10^{18.7} \text{ eV}$ where the spectrum becomes harder [11]. The expected number of CRs observed by GP300 in the ankle energy region should increase accordingly, and the ankle structure will be resolved.

Finally, a very simple prediction of the statistical uncertainty in our future measurement of the mean depth of the air-shower maximum X_{max} is presented. LOFAR estimated the statistical uncertainty in their X_{max} measurement by $\sigma(X_{\text{max}})/\sqrt{N}$, where $\sigma(X_{\text{max}})$ is the standard deviation

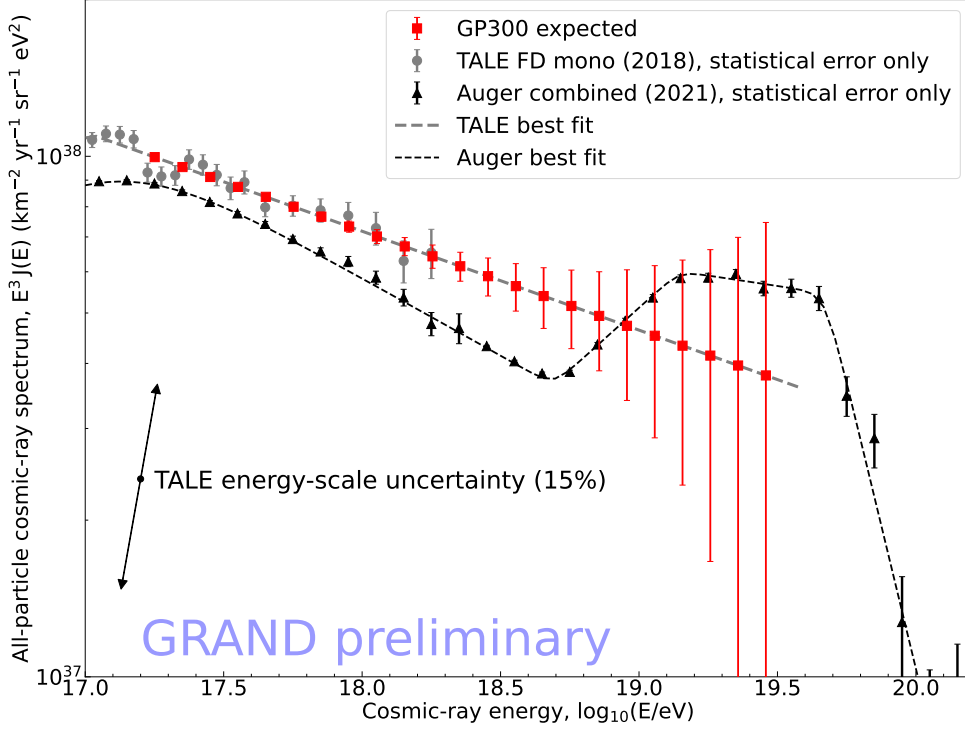


Figure 4: Prediction of the measurement of the CR energy spectrum by GP300 for a one-year observation. The error bars show statistical errors assuming a Poisson distribution. The gray data points show the measurement by the TALE fluorescence detector for 1,080 hours of observation [6]. The gray dashed lines show the best-fit broken power-law function to the TALE measurement; see Equation (1). The black data points are given by the Pierre Auger Observatory, combining the measurements by their surface detector arrays with 750 and 1500 m intervals [8]. The error bars of the TALE and Auger measurements are statistical only, and the systematic uncertainty in the flux normalization from the energy-scale uncertainty is indicated with the arrows for the case of TALE.

of the distribution of X_{\max} in the energy bin of interest and N is the number of events in that energy bin [12]. Assuming similar event-reconstruction performance of GP300 to that of LOFAR and $\sigma(X_{\max}) = 60 \text{ g/cm}^2$ for the whole energy range accounting for the X_{\max} measurement by LOFAR [12], the statistical uncertainty in mean X_{\max} in the measurement by GP300 per energy bin ($\Delta \ln E = 0.1$) is estimated as 0.7, 1.9, and 6.5 g/cm^2 at $10^{17.5}$, 10^{18} , and $10^{18.5} \text{ eV}$, respectively. The prediction of the statistical uncertainty is about five times smaller than those in the previous measurements using radio detectors, LOFAR and AERA [12, 13], at $10^{17.5} \text{ eV}$. Therefore, systematic uncertainties will be a dominant contribution that limits the interpretation of the mean X_{\max} measurement by GP300; for example the systematic uncertainty in the LOFAR measurement is $\approx 7 \text{ g/cm}^2$ [12]. The calibration of the DUs is a crucial work to reduce the systematic uncertainty.

$\log_{10}(E [\text{eV}])$	Expected number of CR events per year
17.2 – 17.3	3821
17.3 – 17.4	8551
17.4 – 17.5	11457
17.5 – 17.6	8436
17.6 – 17.7	6034
17.7 – 17.8	3884
17.8 – 17.9	2402
17.9 – 18.0	1655
18.0 – 18.1	1055
18.1 – 18.2	624
18.2 – 18.3	378
18.3 – 18.4	244
18.4 – 18.5	142
18.5 – 18.6	91
18.6 – 18.7	56
18.7 – 18.8	33
18.8 – 18.9	21
18.9 – 19.0	12
19.0 – 19.1	7
19.1 – 19.2	4
19.2 – 19.3	2
19.3 – 19.4	1
19.4 – 19.5	1

Table 1: Preliminary estimate of the number of CRs to be observed by GP300 in each logarithmic energy bin after one-year observation.

5. Conclusion

This study calculates the exposure of the GP300 radio detector array for CRs above 10^{17} eV. The trigger efficiency of GP300 is 50, 80, and 90% at $10^{17.5}$, $10^{17.9}$, and $10^{18.3}$ eV, respectively. The trigger efficiency improves over the whole energy range above 10^{17} eV with an increase of zenith angle θ in $65^\circ < \theta \lesssim 80^\circ$ due to the large footprint size of the radio emission on the ground. On the other hand, in the higher zenith-angle range in $\theta \gtrsim 80^\circ$, the trigger efficiency becomes smaller in $E \lesssim 10^{18}$ eV due to the attenuation of the radio emission from very inclined showers.

The exposure of GP300 for one-day observation reaches 50, 80, and $90 \text{ km}^2 \text{ day sr}$ at $10^{17.5}$, 10^{18} , and 10^{19} eV, respectively. Based on the calculated exposure, about 130 CR events are expected to be observed per day by GP300 in $E > 10^{17}$ eV and $\theta > 65^\circ$. A total $\simeq 4.9 \times 10^4$ CR events will be observed by GP300 after one-year observation, and the CR energy spectrum will be measured in $10^{17.2} \text{ eV} < E < 10^{19.5} \text{ eV}$ with a high statistical precision; the observation will have about eight and five times more statistics at around $10^{17.5}$ eV and 10^{18} eV, respectively, compared with the previous measurement by the TALE fluorescence detector. Also, in the energy range of

$10^{18} \text{ eV} \lesssim E \lesssim 10^{19} \text{ eV}$, the event statistics estimated for the GP300 observation is comparable with that of the measurement by the Pierre Auger Observatory using the dense surface detector array. Our future observation of mean X_{max} will also have a five times smaller statistical error than previous measurements using radio detectors at $10^{17.5} \text{ eV}$, and our interpretation of the chemical composition of CRs will be limited by systematic errors in our measurement. The observation of GP300 with a high statistical precision will surely help us accurately determine the spectral shape and the chemical composition of CRs in the transition region.

References

- [1] The GRAND Collaboration *Science China Physics, Mechanics & Astronomy* **63** (2019) 219501.
- [2] K. Kotera *et al.* *arXiv.2408.16316* (2024) .
- [3] S. Chiche *et al.* *arXiv.2409.02195* (2024) .
- [4] The GRAND Collaboration *Computer Physics Communications* **308** (2025) 109461.
- [5] T. Huege, M. Ludwig, and W. James *AIP Conf. Proc* **128** (2013) 1535.
- [6] The Telescope Array Collaboration *The Astrophysical Journal* **865** no. 1, (Sep, 2018) 74.
- [7] P. Ma, Y. Zhang, P. Zhang, and X. Xu *PoS(ICRC2025)*453 .
- [8] The Pierre Auger Collaboration *The European Physical Journal C* **81** (2021) 966.
- [9] P. Sokolsky *Nuclear Physics B - Proceedings Supplements* **196** (2009) 67–73. Proceedings of the XV International Symposium on Very High Energy Cosmic Ray Interactions (ISVHECRI 2008).
- [10] The Pierre Auger Collaboration *Phys. Rev. D* **102** (Sep, 2020) 062005.
- [11] A. Coleman, J. Eser, E. Mayotte, F. Sarazin, F. Schröder, *et al.* *Astroparticle Physics* **149** (2023) 102819.
- [12] A. Corstanje, S. Buitink, H. Falcke, B. M. Hare, J. R. Hörandel, *et al.* *Phys. Rev. D* **103** (May, 2021) 102006.
- [13] The Pierre Auger Collaboration *Phys. Rev. D* **109** (Jan, 2024) 022002.

Full Author List: GRAND Collaboration

J. Álvarez-Muñiz¹, R. Alves Batista^{2,3}, A. Benoit-Lévy⁴, T. Bister^{5,6}, M. Bohacova⁷, M. Bustamante⁸, W. Carvalho⁹, Y. Chen^{10,11}, L. Cheng¹², S. Chiche¹³, J. M. Colley³, P. Correa³, N. Cucu Laurenciu^{5,6}, Z. Dai¹¹, R. M. de Almeida¹⁴, B. de Errico¹⁴, J. R. T. de Mello Neto¹⁴, K. D. de Vries¹⁵, V. Decoene¹⁶, P. B. Denton¹⁷, B. Duan^{10,11}, K. Duan¹⁰, R. Engel^{18,19}, W. Erba^{20,21}, Y. Fan¹⁰, A. Ferrière^{4,3}, Q. Gou²², J. Gu¹², M. Guelfand^{3,2}, G. Guo²³, J. Guo¹⁰, Y. Guo²², C. Guépin²⁴, L. Güllow¹⁸, A. Haungs¹⁸, M. Havelka⁷, H. He¹⁰, E. Hivon², H. Hu²², G. Huang²³, X. Huang¹⁰, Y. Huang¹², T. Huege^{25,18}, W. Jiang²⁶, S. Kato², R. Koirala^{27,28,29}, K. Kotera^{2,15}, J. Köhler¹⁸, B. L. Lago³⁰, Z. Lai³¹, J. Lavoisier^{2,20}, F. Legrand³, A. Leisos³², R. Li²⁶, X. Li²², C. Liu²², R. Liu^{28,29}, W. Liu²², P. Ma¹⁰, O. Macías^{31,33}, F. Magnard², A. Marcowith²⁴, O. Martineau-Huynh^{3,12,2}, Z. Mason³¹, T. McKinley³¹, P. Minodier^{20,2,21}, M. Mostafa³⁴, K. Murase^{35,36}, V. Niess³⁷, S. Nonis³², S. Ogio^{21,20}, F. Oikonomou³⁸, H. Pan²⁶, K. Papageorgiou³⁹, T. Pierog¹⁸, L. W. Piotrowski⁹, S. Prunet⁴⁰, C. Prévotat², X. Qian⁴¹, M. Roth¹⁸, T. Sako^{21,20}, S. Shinde³¹, D. Szálas-Motesiczky^{5,6}, S. Ślawiński⁹, K. Takahashi²¹, X. Tian⁴², C. Timmermans^{5,6}, P. Tobiska⁷, A. Tsirigotis³², M. Tüeros⁴³, G. Vittakis³⁹, V. Voisin³, H. Wang²⁶, J. Wang²⁶, S. Wang¹⁰, X. Wang^{28,29}, X. Wang⁴¹, D. Wei¹⁰, F. Wei²⁶, E. Weissling³¹, J. Wu²³, X. Wu^{12,44}, X. Wu⁴⁵, X. Xu²⁶, X. Xu^{10,11}, F. Yang²⁶, L. Yang⁴⁶, X. Yang⁴⁵, Q. Yuan¹⁰, P. Zarka⁴⁷, H. Zeng¹⁰, C. Zhang^{42,48,28,29}, J. Zhang¹², K. Zhang^{10,11}, P. Zhang²⁶, Q. Zhang²⁶, S. Zhang⁴⁵, Y. Zhang¹⁰, H. Zhou⁴⁹

¹Departamento de Física de Partículas & Instituto Galego de Física de Altas Enerxías, Universidade de Santiago de Compostela, 15782 Santiago de Compostela, Spain

²Institut d'Astrophysique de Paris, CNRS UMR 7095, Sorbonne Université, 98 bis bd Arago 75014, Paris, France

³Sorbonne Université, Université Paris Diderot, Sorbonne Paris Cité, CNRS, Laboratoire de Physique Nucléaire et de Hautes Energies (LPNHE), 4 Place Jussieu, F-75252, Paris Cedex 5, France

⁴Université Paris-Saclay, CEA, List, F-91120 Palaiseau, France

⁵Institute for Mathematics, Astrophysics and Particle Physics, Radboud Universiteit, Nijmegen, the Netherlands

⁶Nikhef, National Institute for Subatomic Physics, Amsterdam, the Netherlands

⁷Institute of Physics of the Czech Academy of Sciences, Na Slovance 1999/2, 182 00 Prague 8, Czechia

⁸Niels Bohr International Academy, Niels Bohr Institute, University of Copenhagen, 2100 Copenhagen, Denmark

⁹Faculty of Physics, University of Warsaw, Pasteura 5, 02-093 Warsaw, Poland

¹⁰Key Laboratory of Dark Matter and Space Astronomy, Purple Mountain Observatory, Chinese Academy of Sciences, 210023 Nanjing, Jiangsu, China

¹¹School of Astronomy and Space Science, University of Science and Technology of China, 230026 Hefei Anhui, China

¹²National Astronomical Observatories, Chinese Academy of Sciences, Beijing 100101, China

¹³Inter-University Institute For High Energies (IIHE), Université libre de Bruxelles (ULB), Boulevard du Triomphe 2, 1050 Brussels, Belgium

¹⁴Instituto de Física, Universidade Federal do Rio de Janeiro, Cidade Universitária, 21.941-611- Ilha do Fundão, Rio de Janeiro - RJ, Brazil

¹⁵IIHE/ELEM, Vrije Universiteit Brussel, Pleinlaan 2, 1050 Brussels, Belgium

¹⁶SUBATECH, Institut Mines-Télécom Atlantique, CNRS/IN2P3, Université de Nantes, Nantes, France

¹⁷High Energy Theory Group, Physics Department Brookhaven National Laboratory, Upton, NY 11973, USA

¹⁸Institute for Astroparticle Physics, Karlsruhe Institute of Technology, D-76021 Karlsruhe, Germany

¹⁹Institute of Experimental Particle Physics, Karlsruhe Institute of Technology, D-76021 Karlsruhe, Germany

²⁰ILANCE, CNRS – University of Tokyo International Research Laboratory, Kashiwa, Chiba 277-8582, Japan

²¹Institute for Cosmic Ray Research, University of Tokyo, 5 Chome-1-5 Kashiwanoha, Kashiwa, Chiba 277-8582, Japan

²²Institute of High Energy Physics, Chinese Academy of Sciences, 19B YuquanLu, Beijing 100049, China

²³School of Physics and Mathematics, China University of Geosciences, No. 388 Lumo Road, Wuhan, China

²⁴Laboratoire Univers et Particules de Montpellier, Université Montpellier, CNRS/IN2P3, CC72, Place Eugène Bataillon, 34095, Montpellier Cedex 5, France

²⁵Astrophysical Institute, Vrije Universiteit Brussel, Pleinlaan 2, 1050 Brussels, Belgium

²⁶National Key Laboratory of Radar Detection and Sensing, School of Electronic Engineering, Xidian University, Xi'an 710071, China

²⁷Space Research Centre, Faculty of Technology, Nepal Academy of Science and Technology, Khumaltar, Lalitpur, Nepal

²⁸School of Astronomy and Space Science, Nanjing University, Xianlin Road 163, Nanjing 210023, China

²⁹Key laboratory of Modern Astronomy and Astrophysics, Nanjing University, Ministry of Education, Nanjing 210023, China

³⁰Centro Federal de Educação Tecnológica Celso Suckow da Fonseca, UnED Petrópolis, Petrópolis, RJ, 25620-003, Brazil

³¹Department of Physics and Astronomy, San Francisco State University, San Francisco, CA 94132, USA

³²Hellenic Open University, 18 Aristotelous St, 26335, Patras, Greece

³³GRAPPA Institute, University of Amsterdam, 1098 XH Amsterdam, the Netherlands

³⁴Department of Physics, Temple University, Philadelphia, Pennsylvania, USA

³⁵Department of Astronomy & Astrophysics, Pennsylvania State University, University Park, PA 16802, USA

³⁶Center for Multimessenger Astrophysics, Pennsylvania State University, University Park, PA 16802, USA

³⁷CNRS/IN2P3 LPC, Université Clermont Auvergne, F-63000 Clermont-Ferrand, France

³⁸Institutt for fysikk, Norwegian University of Science and Technology, Trondheim, Norway

³⁹Department of Financial and Management Engineering, School of Engineering, University of the Aegean, 41 Kountouriotou Chios,

Northern Aegean 821 32, Greece

⁴⁰Laboratoire Lagrange, Observatoire de la Côte d’Azur, Université Côte d’Azur, CNRS, Parc Valrose 06104, Nice Cedex 2, France

⁴¹Department of Mechanical and Electrical Engineering, Shandong Management University, Jinan 250357, China

⁴²Department of Astronomy, School of Physics, Peking University, Beijing 100871, China

⁴³Instituto de Física La Plata, CONICET - UNLP, Boulevard 120 y 63 (1900), La Plata - Buenos Aires, Argentina

⁴⁴Shanghai Astronomical Observatory, Chinese Academy of Sciences, 80 Nandan Road, Shanghai 200030, China

⁴⁵Purple Mountain Observatory, Chinese Academy of Sciences, Nanjing 210023, China

⁴⁶School of Physics and Astronomy, Sun Yat-sen University, Zhuhai 519082, China

⁴⁷LIRA, Observatoire de Paris, CNRS, Université PSL, Sorbonne Université, Université Paris Cité, CY Cergy Paris Université, 92190 Meudon, France

⁴⁸Kavli Institute for Astronomy and Astrophysics, Peking University, Beijing 100871, China

⁴⁹Tsung-Dao Lee Institute & School of Physics and Astronomy, Shanghai Jiao Tong University, 200240 Shanghai, China

Acknowledgments

The GRAND Collaboration is grateful to the local government of Dunhuang during site survey and deployment approval, to Tang Yu for his help on-site at the GRANDProto300 site, and to the Pierre Auger Collaboration, in particular, to the staff in Malargüe, for the warm welcome and continuing support. The GRAND Collaboration acknowledges the support from the following funding agencies and grants. **Brazil:** Conselho Nacional de Desenvolvimento Científico e Tecnológico (CNPq); Fundação de Amparo à Pesquisa do Estado de Rio de Janeiro (FAPERJ); Coordenação Aperfeiçoamento de Pessoal de Nível Superior (CAPES). **China:** National Natural Science Foundation (grant no. 12273114); NAOC, National SKA Program of China (grant no. 2020SKA0110200); Project for Young Scientists in Basic Research of Chinese Academy of Sciences (no. YSBR-061); Program for Innovative Talents and Entrepreneurs in Jiangsu, and High-end Foreign Expert Introduction Program in China (no. G2023061006L); China Scholarship Council (no. 202306010363); and special funding from Purple Mountain Observatory. **Denmark:** Villum Fonden (project no. 29388). **France:** “Emergences” Programme of Sorbonne Université; France-China Particle Physics Laboratory; Programme National des Hautes Energies of INSU; for IAP—Agence Nationale de la Recherche (“APACHE” ANR-16-CE31-0001, “NUTRIG” ANR-21-CE31-0025, ANR-23-CPJ1-0103-01), CNRS Programme IEA Argentine (“ASTRONU”, 303475), CNRS Programme Blanc MITI (“GRAND” 2023.1 268448), CNRS Programme AMORCE (“GRAND” 258540); Fulbright-France Programme; IAP+LPNHE—Programme National des Hautes Energies of CNRS/INSU with INP and IN2P3, co-funded by CEA and CNES; IAP+LPNHE+KIT—NuTRIG project, Agence Nationale de la Recherche (ANR-21-CE31-0025); IAP+VUB: PHC TOURNESOL programme 48705Z. **Germany:** NuTRIG project, Deutsche Forschungsgemeinschaft (DFG, Projektnummer 490843803); Helmholtz—OCPC Postdoc-Program. **Poland:** Polish National Agency for Academic Exchange within Polish Returns Program no. PPN/PPO/2020/1/00024/U/00001,174; National Science Centre Poland for NCN OPUS grant no. 2022/45/B/ST2/0288. **USA:** U.S. National Science Foundation under Grant No. 2418730. Computer simulations were performed using computing resources at the CCIN2P3 Computing Centre (Lyon/Villeurbanne, France), partnership between CNRS/IN2P3 and CEA/DSM/Irfu, and computing resources supported by the Chinese Academy of Sciences.